Electronic Supplementary Material (ESI) for Chemical Communications.

Supplementary Information

Peak-differentiation-imitating-assisted SERS strategy for accurate detection of estrogens at femtomole level

Xinyu Wang, ‡ Mengxiang Song, ‡ Yuhong Wang, * Wei Deng and Dan Li *

School of Chemical and Environmental Engineering, Shanghai Institute of Technology, Shanghai 201418, P. R. China. E-mail: dany@sit.edu.cn

*To whom the correspondence should be addressed. E-mail: dany@sit.edu.cn

‡These authors contributed equally to this work.

Experimental section

Materials. Estrone (E1, 99%), 17β-estradiol (E2, 99%), estriol (E3, 98%), p-aminothiophenol (PATP, 99.9%), chloroauric acid ($HAuCl_4$, 99.0%), silver nitrite ($AgNO_3$, ≥99.0%), trisodium citrate ($Na_3C_6H_5O_7$, 99.5%), 2-aminoterephthalic acid (APA, 99%) and α-carboxyl-ω-mercapto poly (ethylene glycol) (CPEG-SH) were provided by Titan-Reagent Co., Ltd. (Shanghai, China). Human serum (ERMDA474IFCC), bovine serum albumin (BSA, ≥98%), estradiol benzoate, and nilestriol were purchased from Shanghai Reagent Company. Deionized-water with a conductivity of 18.2 MΩ·cm was utilized throughout this study.

Synthesis of PEG-modified silver seeds. Ag seeds were prepared in aqueous solution using the method described previously. [1] Specifically, a silver nitrate stock solution (0.56 mM) was first prepared by dissolving 9.52 mg (0.056 mmol) of $AgNO_3$ in 100 mL of deionized water, and 20 mL of trisodium citrate (12.9 mg, 0.50 mmol) was added dropwise under stirring. Then, 0.50 mL of 0.01 M freshly prepared sodium borohydride ($NaBH_4$) was added to the mixture and the color of solution changed from colorless to yellow. The as-synthesized Ag seeds were used 2 h after preparation but cannot be used after 5 h.

PEG-modified Ag seeds were obtained by a ligand exchange procedure. Specifically, 10 mL of Ag seeds colloids were centrifuged at 8,500 rpm for 10 min to remove citrate in the solution. The precipitate was then re-dispersed in water (10 mL), and subsequently 0.5 mL of 10 mM CPEG-SH was added dropwise under vigorous stirring. Excess CPEG-SH was removed by centrifugation at 8,000 rpm for 10 min. The concentration of PEG-modified Ag seeds was estimated according to the concentration of Ag seeds based on the Lambert-Beer law.

Preparation of plasmonic MIL-101(Fe) nanoparticles (PMNs). AgNPs@MIL-101(Fe) core-shell nanoparticles (PMNs) were synthesized using a self-assembled strategy. Specifically, 5.0 mL of PEG-modified silver seeds was dispersed in 10 mL of deionized water and then placed in a Teflon-coated stainless-steel cylinder. Next, 0.635 g of $FeCl_3$, 0.208 g of APA ligands and 0.106 g of $Na_3C_6H_5O_7$ were added into the mixture under stirring. The resultant mixtures were heated at 80 ℃ for 10 h. The impurities were removed by washing with DMF and ethanol for several times. The resultant PMNs was centrifuged and then dried overnight at 60 ℃ under vacuum. The concentration of PMNs (~ 0.5 nM) was estimated according to the Lambert-Beer law. [2]

SERS measurement on the PMNs. The PATP-modified PMNs were synthesized by a self-assembly procedure. Specifically, 10 μL of PATP (0.1 μM) was mixed with 1 mL of PMNs dispersions (0.5 nM). Non-bound PATP was eradicated by centrifugation at 8,000 rpm for 5 min. The resultant precipitates were dispersed in water and stored at room temperature. For the first step diazotization reaction, 10 μL of sodium nitrite (0.5 μM) containing 0.15 M PBS (pH 6.0) was added into PMNs colloids. After reaction for 2 min, the resulting PMNs were subsequently mixed

with E1, E2 and E3 following the same procedure to create azo dyes. After the Griess reaction, 5 μL of the mixture was transferred onto hydrophobicity-modified Si substrates, and SERS spectrum was recorded. SERS measurement was conducted on a BAC151B micro-Raman system with a 785 nm laser (15 mW). The accumulation time for each SERS analysis was 20s with 3 lots of data accumulation.

Peak differentiation and peak imitating. The peak-fitting procedures were carried out using the linear progressive baseline correction option of PeakFit 4.12 and an exponentially-modified Lorentzian fit. The number of fitted PEs peaks was accorded to the DFT-simulated spectrum and literature-related peak data. To develop a reliable SERS method for PEs detection, additional PATP peaks were involved in the deconvolutions, using the peak-position and full widths at half-maxima (fwhm) obtained from a PATP-capped PMNs as a reference. To avoid spectra overfit, we fixed the peak position and fwhm during spectral deconvolutions, utilizing the fwhm of PATP-modified PMNs peaks as a guideline.

Discrimination and detection of PEs in actual specimens. Hospital wastewater were selected as complex matrices. PTFE membrane with a pore size of 0.1 μm was employed for removing indissoluble solid matter from wastewater specimens. Milk, duck, and fish samples were obtained from a local supermarket. 10 mL of H_2O_2/HNO_3 (2:8) was used for extraction of 0.1 g of homogenized samples in 20 mL centrifugal tubes. Then the mixture was transferred to 50 mL beaker and heated nearly to dryness. Afterward, the solution was spiked with different PEs concentrations. Prior to the detection of PEs, 1 mL of PATP-capped PMNs (0.5 nM) containing 0.15 M PBS (pH 6.0) and 0.5 μM sodium nitrite was incubated with the extracted solutions for 3 min at 25 ± 2 ℃. The resultant solution was analyzed by SERS spectra.

Raman enhancement factor. The enhancement factor (EF) can be calculated using the following formula:

$$EF=(I_{SERS}/I_{bulk})\times(N_{bulk}/N_{SERS}) \quad (1)$$

$$N_{SERS}=N_{PATP}S_{Laser} \quad (2)$$

$$N_{bulk}=CVN_AS_{Laser}/S_{bulk} \quad (3)$$

where I_{SERS} and I_{bulk} are the vibration intensities in the SERS of p-aminothiophenol (PATP) and normal Raman spectra of PATP, respectively. N_{bulk} and N_{SERS} are the numbers of PATP molecules under laser illumination for the bulk specimen, and the numbers of PATP molecules on the PMNs, respectively. The number of PATP molecules was calculated using equation S2 and S3, where C is the molar concentration of the PATP solution, V is the volume of a droplet, N_A is the Avogadro constant (6.02×10^{23} mol^{-1}). S_{Laser} and S_{bulk} are laser spot size and the area of the PATP solution dropped on the silicon wafer ($\pi\times(0.1/2)^2 cm^2 = 0.008$ cm^2). In the experiment, 20 μL of PATP solution (1.0 $mol\cdot L^{-1}$) was dried onto the Si wafer (d_{PATP}=1 mm) and thus N_{bulk} can be estimated as: $N_{bulk} = CVN_AS_{Laser}/S_{bulk} = [(20\ \mu L\times1.0\ mol\cdot L^{-1}\times6.02\times10^{23}\ mol^{-1})/0.008\ cm^2]\times S_{Laser} = 1.5\times10^{13}\ \mu m^{-2}\times S_{Laser}$.

N_{SERS} is determined by laser spot illuminating on the sample and density of PATP molecule adsorbed on the surface of AgNPs. According to the statistical data, the surface area of single AgNPs is about 1256 nm^2 ($\pi \times 400$ nm^2=1256 nm^2). The surface area of the PATP molecule (S_{PATP}) is approximately 0.2 nm^2, so the number of PATP molecules adsorbed by one AgNPs is about 6280 [N_{PATP}=1256/0.2=6280]. There are approximately 796 AgNPs per square micron (N_{AgNPs} = (1/1256) $\times 10^6$ μm^{-2}=796 μm^{-2}), and thus N_{SERS} can be estimated as: $N_{SERS} = S_{Laser} \times 796\ \mu m^{-2} \times 6280 = 5.0 \times 10^6\ \mu m^{-2} \times S_{Laser}$.

I_{SERS} and I_{bulk} were obtained on the peak intensity at 1431 cm^{-1} in SERS spectrum and normal Raman spectrum as shown in Fig. S5, I_{SERS}=12638 and I_{bulk}=29. Substituting these values of into equation S1, EF can be calculated to be around 1.3×10^9 ($12638/29 \times [1.5 \times 10^{13} / (5.0 \times 10^6)] = 1.3 \times 10^9$).

DFT calculations. All-electron DFT calculations have been carried out by the latest version of ORCA quantum chemistry software (Version 5.0.1). The corrected version of B97 exchange-correlation functional proposed by Grimme (B97-3c) was utilized for all calculations. The B97-3c functional which is based on the well-known B97 functional, is a highly efficient method which exploits three corrections: the D3BJ method including three-body term to account for long-range dispersion interactions, a short-range bond-length correction which corrects for systematically overestimated covalent bond-lengths for electronegative elements and a modified stripped-down triple-ζ basis to obtain accurate geometries and relative energies. The nature of noncovalent interaction was studied by using IGM method through Multiwfn software. [3] The visualization of IGM and orbitals were rendered by VMD. The binding energy between PEs and APA was calculated by the following formula: [4]

$$E_{binding} = E_{complex} - (E_{PEs} + E_{APA})$$

Finite-difference time domain (FDTD) simulation. The electric-field simulation was performed on the finite-element-method solver in COMSOL Multiphysics in the frequency domain. The dielectric constants of MIL-101 and AgNPs were adopted from references. [5, 6] The mode of PMNs was constructed according to the corresponding TEM image. The diameter of AgNPs is set as 50 nm. The inter-particle distance between AgNPs is 5 nm. The perfect matched layer was obtained by truncating the simulation area and absorbing the reflected wave. The polarization of the incident light is along the horizontal direction (indicated in the figures). The surrounding medium for both MIL-101, AgNPs and PMNs is air, and the refractive index was taken to be 1.0 for the calculations.

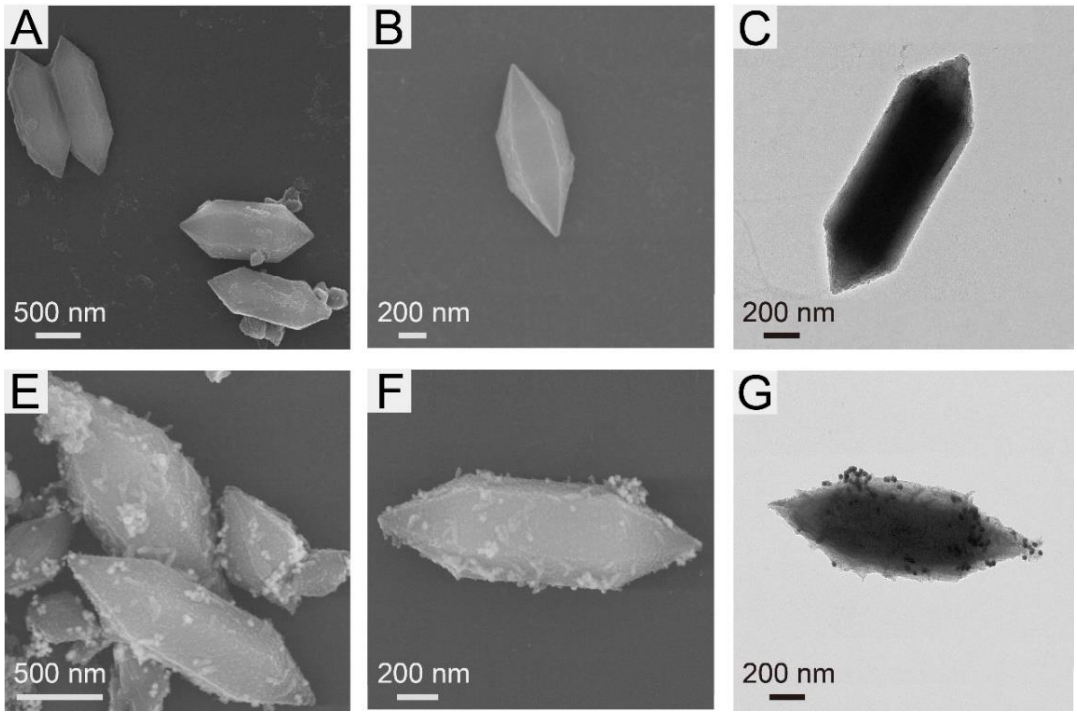

Fig. S1 SEM images and TEM images of the as-synthesized (A-C) MIL-101 and (E-G) PMNs.

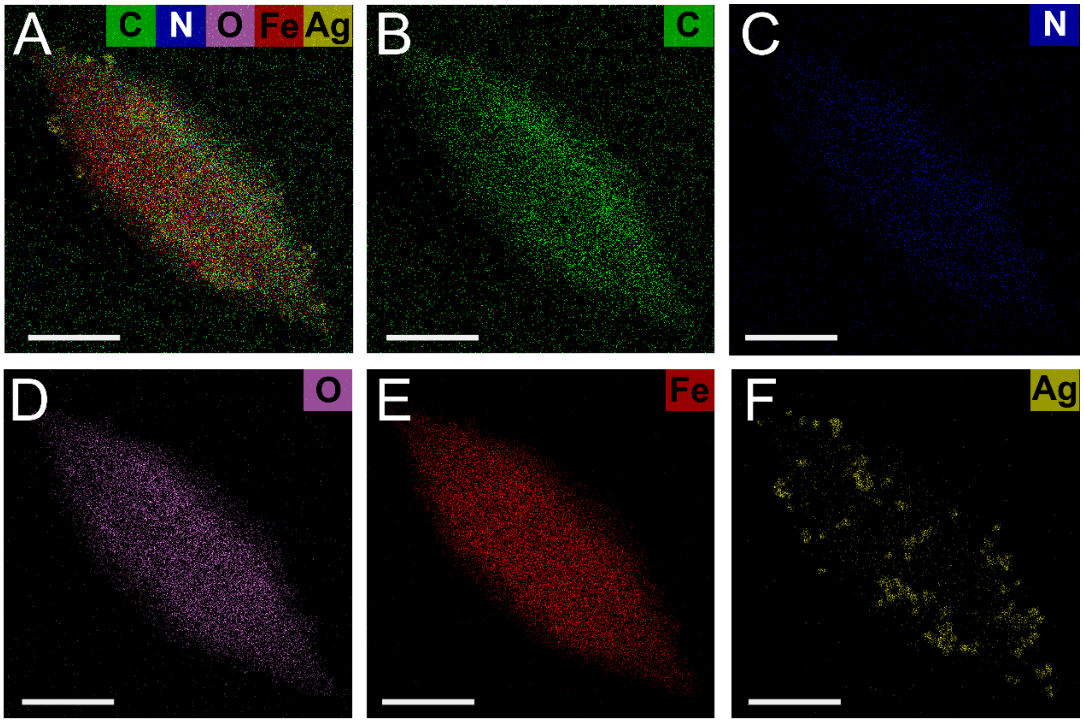

Fig. S2 Corresponding EDS elemental mappings of PMNs. The scale bar is 200 nm.

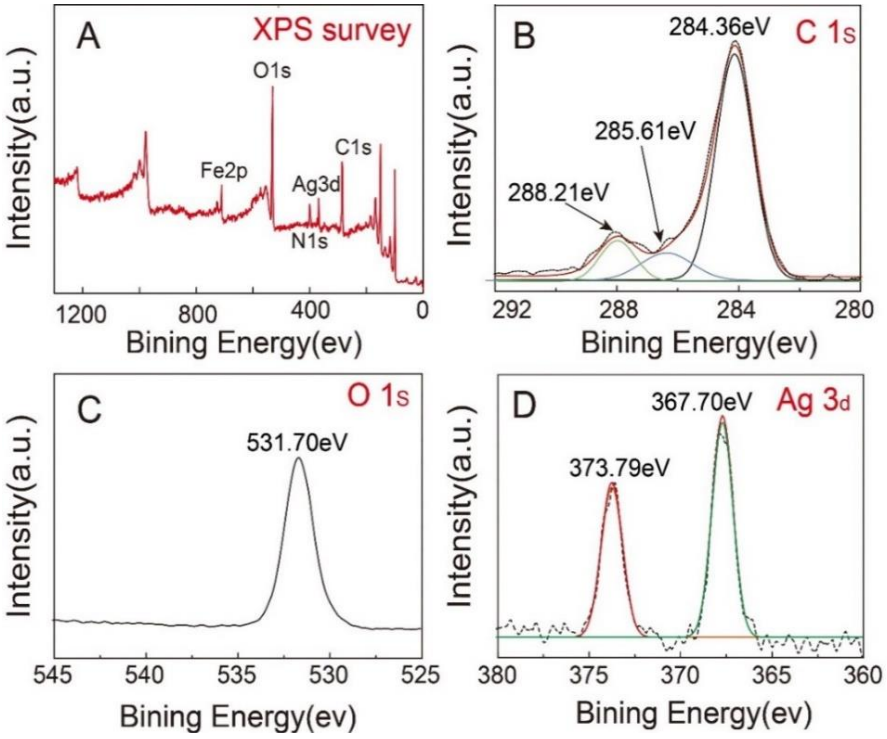

Fig. S3 (A) XPS survey spectra and high-resolution XPS spectra of (B) C1s, (C) O1s and (D) Ag 3d of the PMNs.

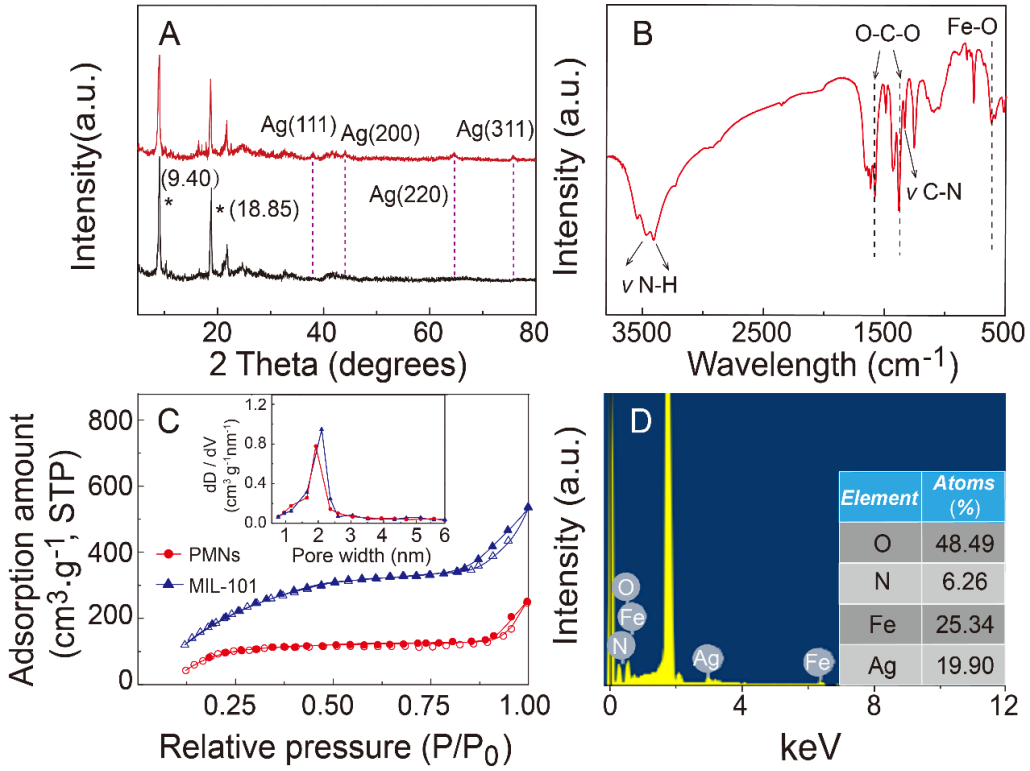

Fig. S4 (A) XRD patterns of MIL-101 (black) and PMNs (red). The asterisks represent the characteristic peaks of MIL-101. (B) FTIR spectra of PMNs. (C) N_2 isotherm for MIL-101 (red) and PMNs (blue) at 77 K. The inset is the differential pore size distributions of MIL-101 and PMNs. (D) EDX spectra of PMNs.

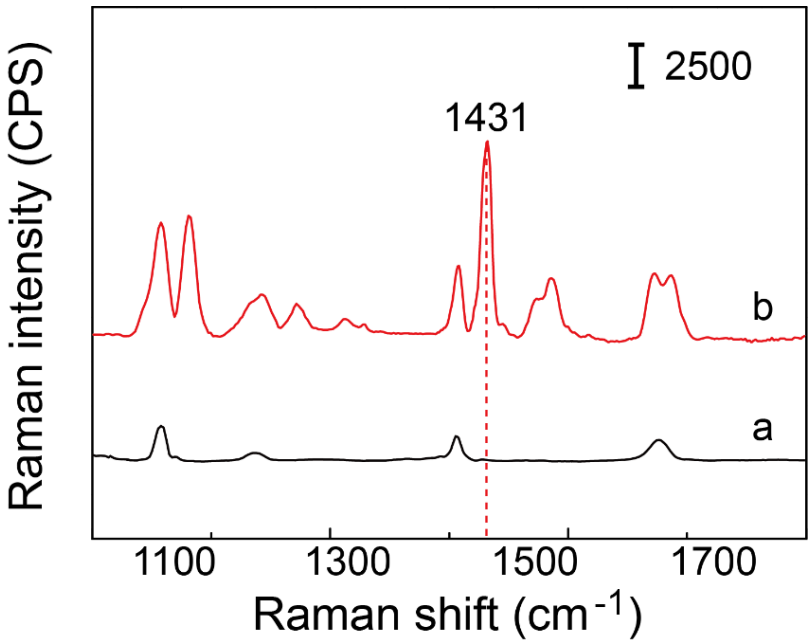

Fig. S5 (a) Normal Raman spectrum of 0.5 M PATP. (b) SERS spectrum of E1 (1 nM) on the surface of PMNs.

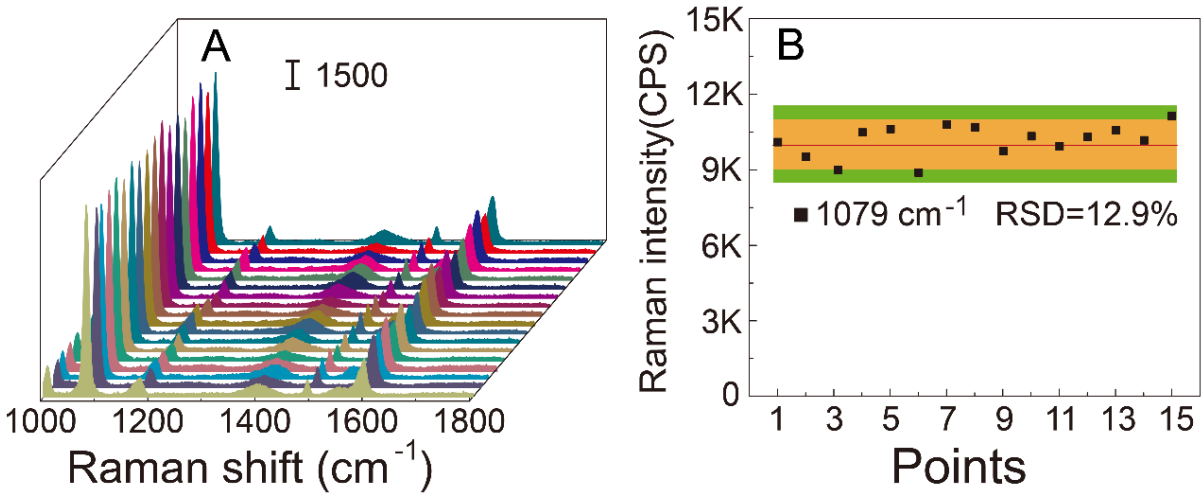

Fig. S6 (A) SERS spectra of PMNs with the presence of PATP (1 μM) in the 15 different positions of the same substrates. (B) SERS intensities distributions of the 1079 cm^{-1} as shown in part (A). The average intensities of 15 spectra are indicated by the red line, intensity variations of ±10% and ±15% are indicated by the orange and green zones, respectively.

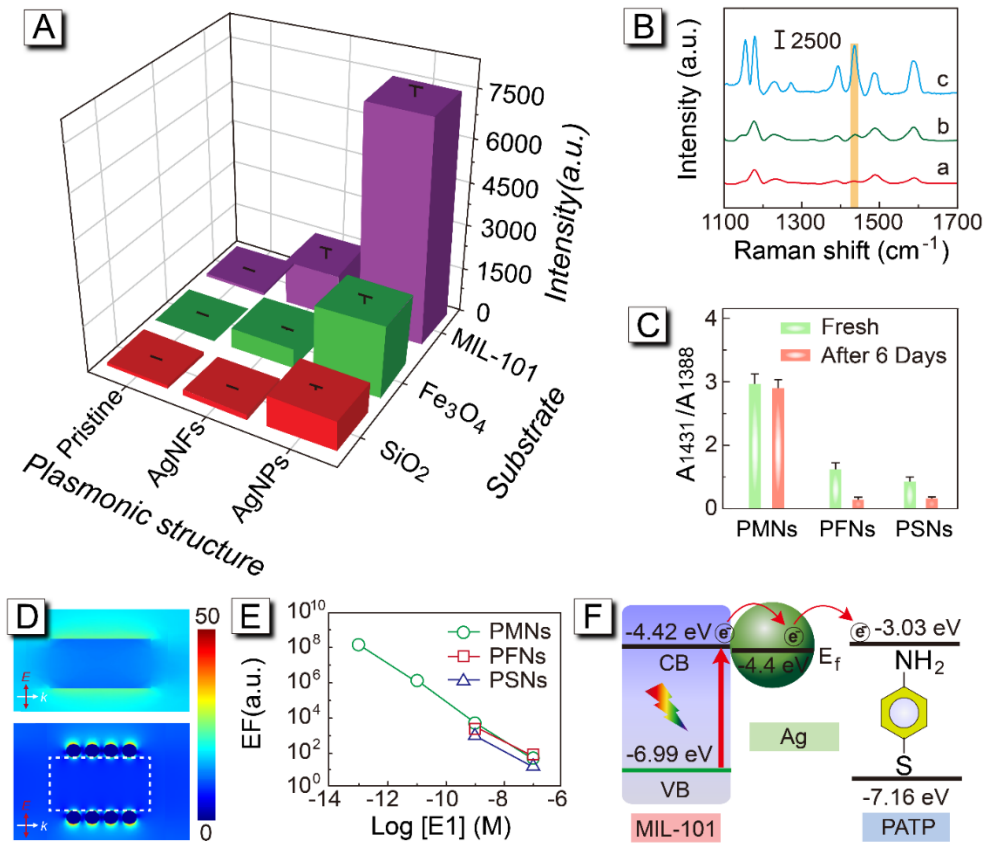

Fig. S7 (A) Comparison of the Raman intensities at 1431 cm^{-1} of E1 (1 nM) absorbed on various substrates. (B) SERS spectra of E1 (1 nM) acquired on (a) AgNPs-capped SiO_2 (PSNs), (b) AgNPs-modified Fe_3O_4 (PFNs) and (c) PMNs. (C) Comparison of the stability of as-synthesized PMNs, PFNs and PSNs. N=N stretching at 1431 cm^{-1} is employed as the indicator. (D) The distribution of surface electric field for single MIL-101 (upper) and PMNs (lower). The white line represents the outer boundary of MIL-101 layer. (E) Calculated EF using an intensity at 1431 cm^{-1} for various substrates. (F) Schematic energy-level diagram of PATP on the PMNs structure with respect to the vacuum level.

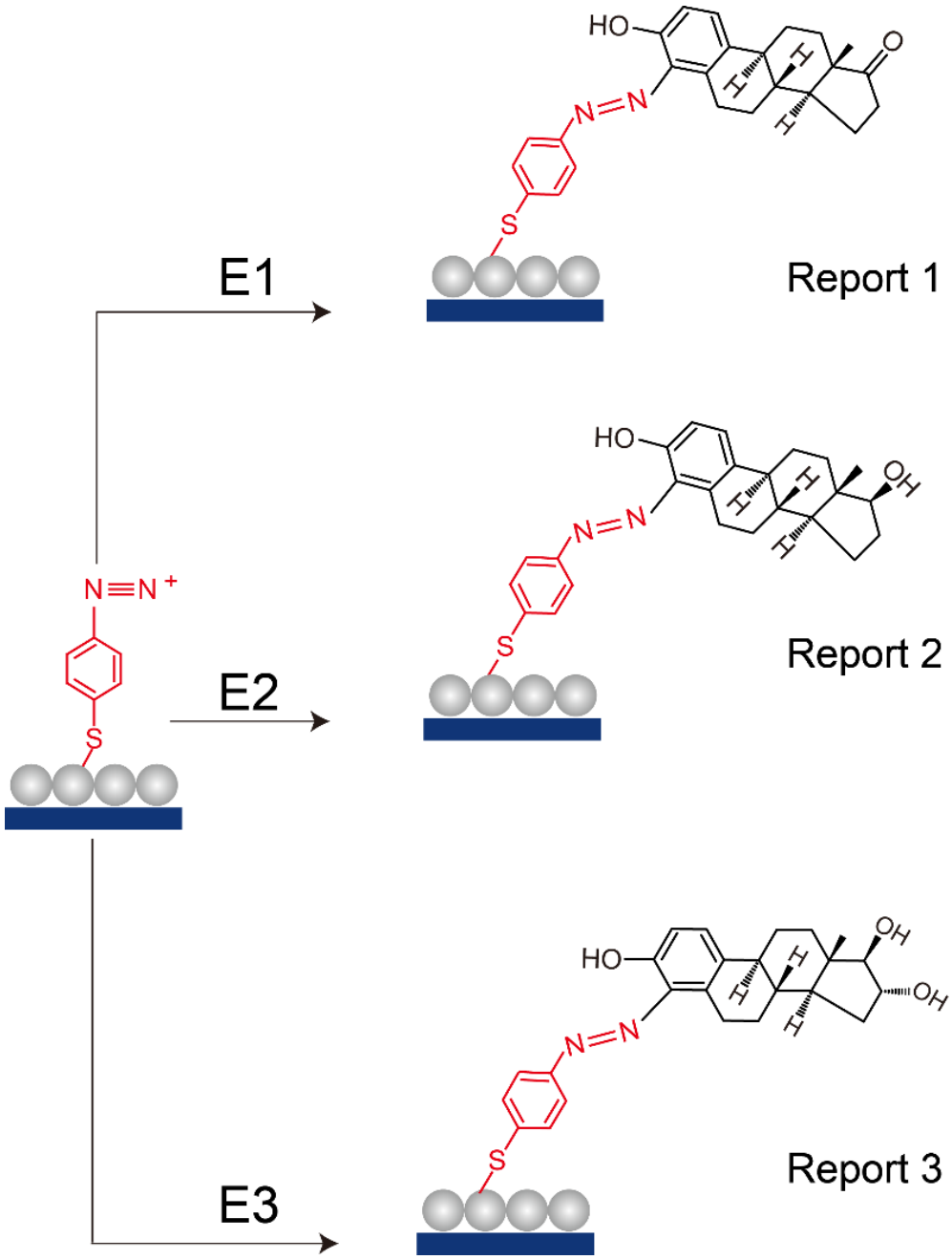

Fig. S8 Scheme for SERS differentiation of estrone (E1), 17β-estradiol (E2) and estriol (E3) based on Griess-reaction between diazonium ions and estrogens using PMNs.

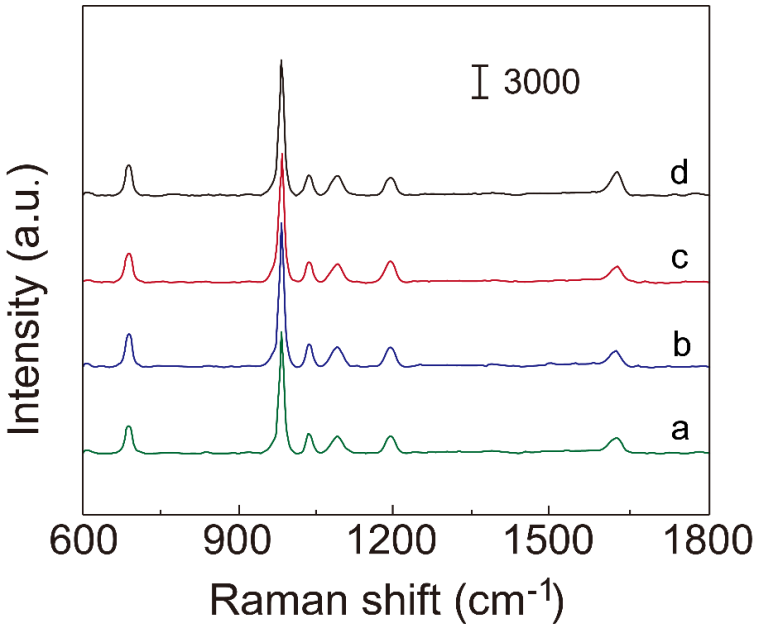

Fig. S9 SERS spectra of (a) 4-mercaptopyridine (Mpy) modified PMNs, and the Mpy-modified PMNs with the presence of (b) estrone (E1), (c) 17β-estradiol (E2) and (d) estriol (E3). There is no difference between four spectra, indicating that the amino group is necessary for specific binding of PEs.

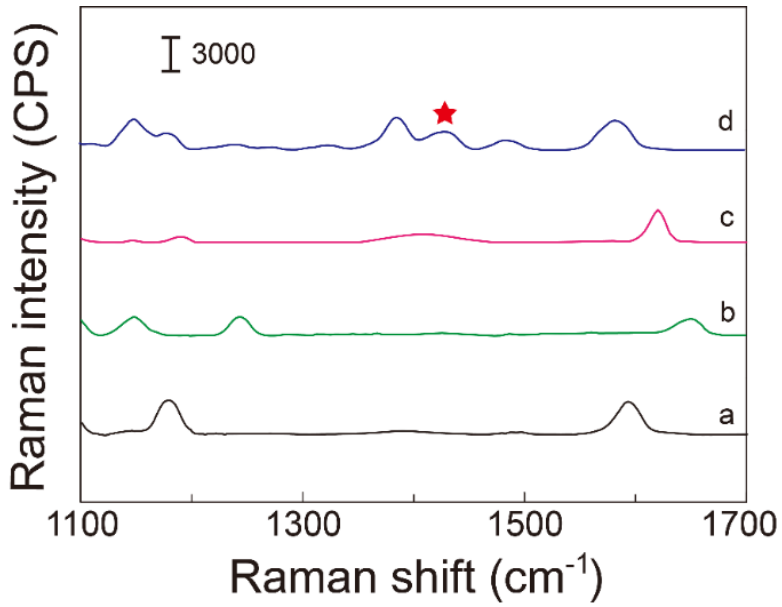

Fig. S10 SERS response of Raman-active linker molecules to E1. PMNs were individually modified with (a) thiophenol, (b) 4-mercaptopyridine, (c) 4-mercaptobenzoic acid and (d) PATP. There are no discernible SERS signals of $\nu_{(N=N)}$ are identified for a, b and c, indicating that the amino group is necessary for specific binding of E1. The red label indicates the N=N stretching mode.

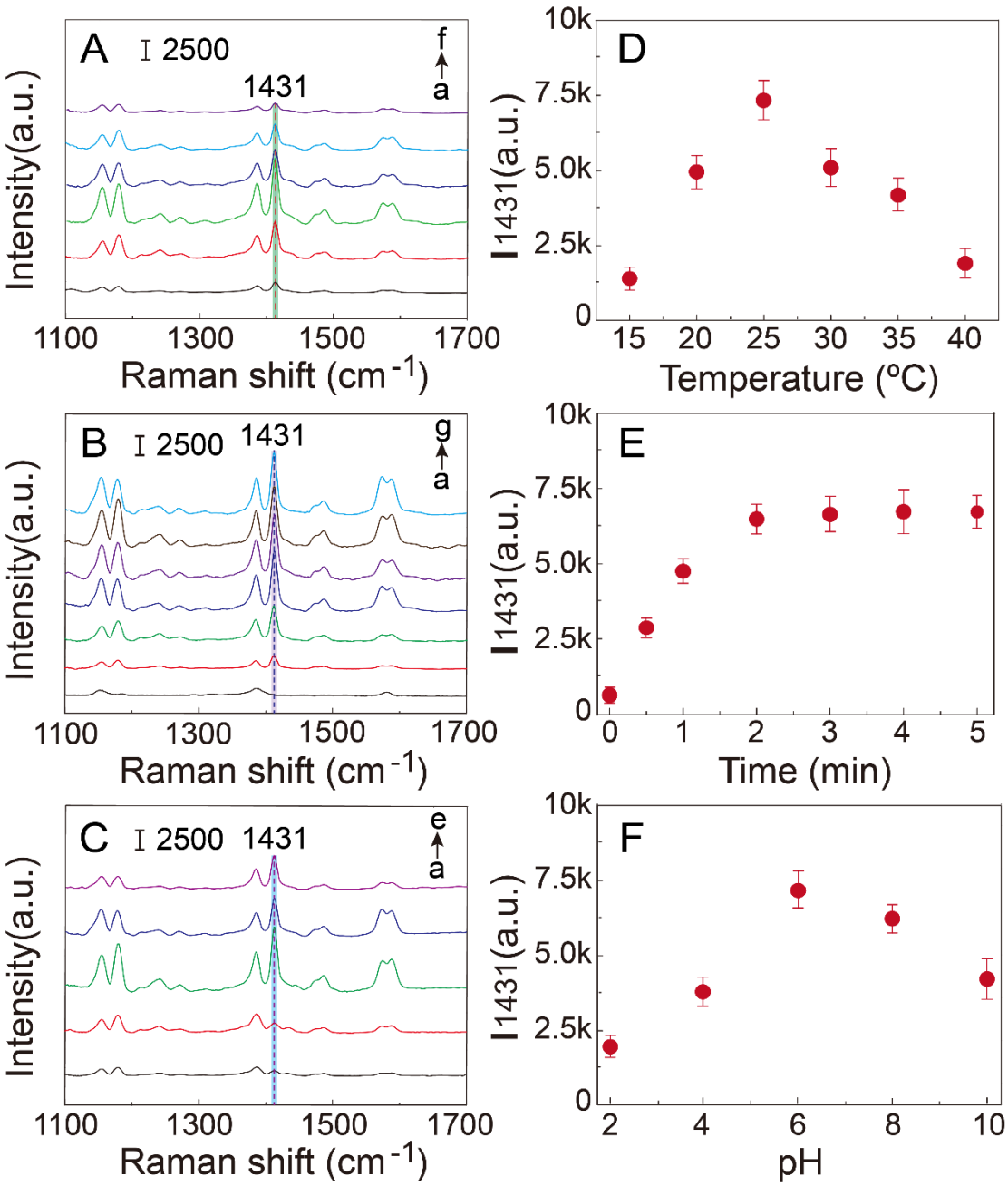

Fig. S11 The effects of (A) incubation temperature (a-f: 15-40 ℃), (B) reaction time (a-g: 0-10 min) and (C) pH (a-e: 2-10) on the SERS performance PMNs toward E1 (1 nM). SERS intensities at 1431 cm^{-1} with different (D) temperature, (E) reaction time and (F) pH. Each data point represents the average value from three measurements on the same samples. Error bars show the standard deviations.

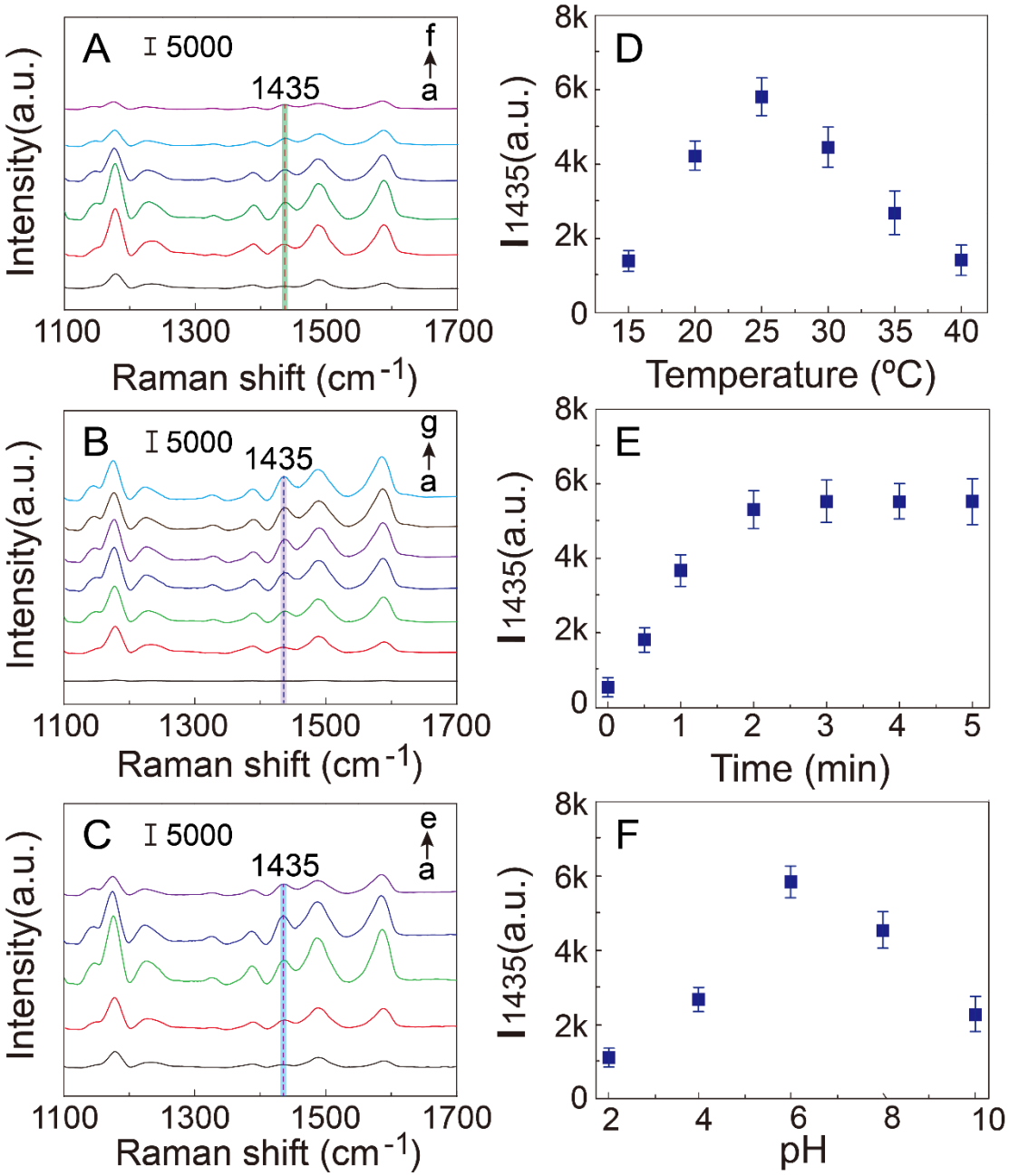

Fig. S12 The effects of (A) incubation temperature (a-f: 15-40 ℃), (B) reaction time (a-g: 0-10 min) and (C) pH (a-e: 2-10) on the SERS performance PMNs toward E2 (1 nM). SERS intensities at 1435 cm^{-1} with different (D) temperature, (E) reaction time and (F) pH. Each data point represents the average value from three measurements on the same samples. Error bars show the standard deviations.

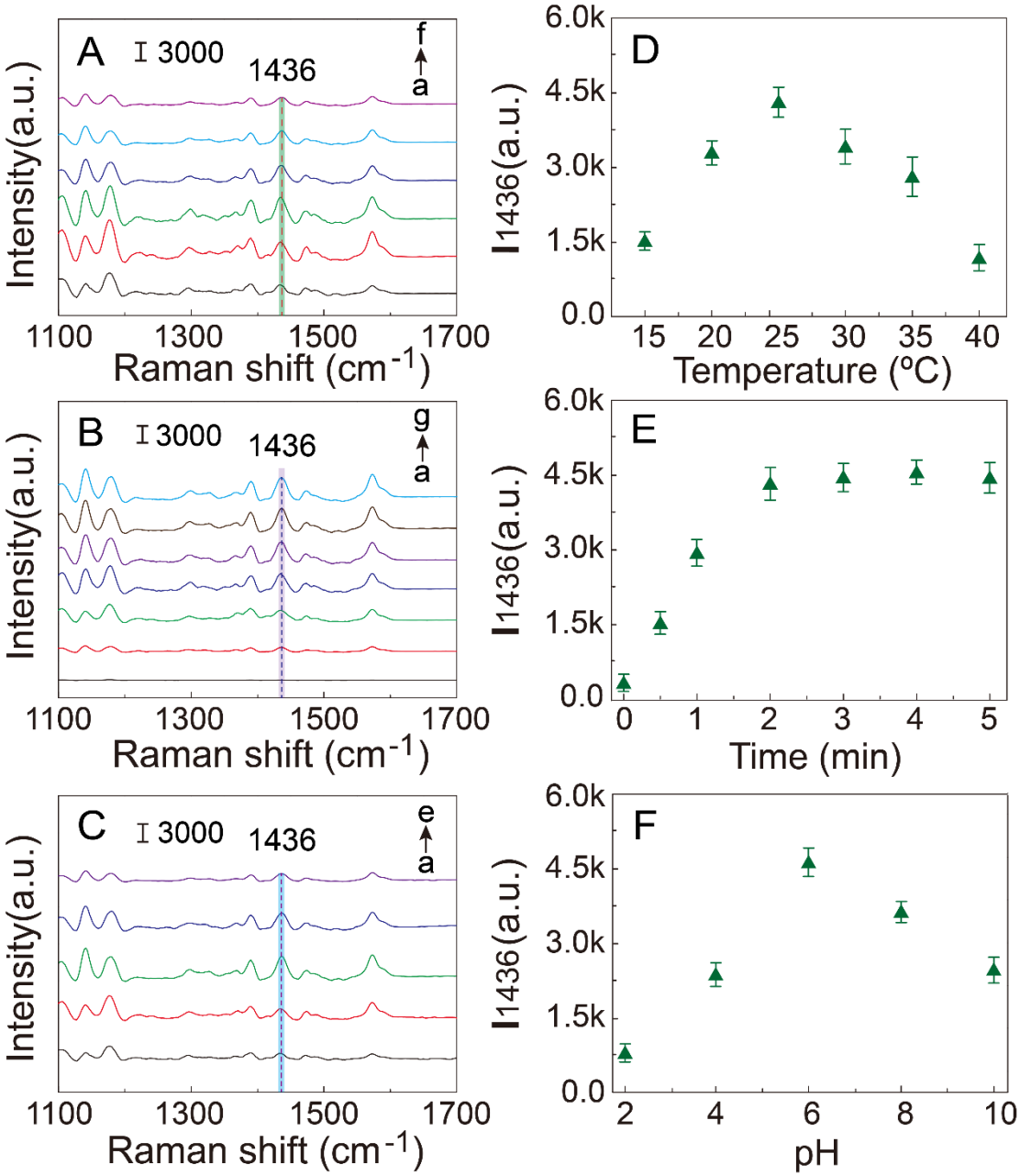

Fig. S13 The effects of (A) incubation temperature (a-f: 15-40 ℃), (B) reaction time (a-g: 0-10 min) and (C) pH (a-e: 2-10) on the SERS performance PMNs toward E3 (1 nM). SERS intensities at 1436 cm^{-1} with different (D) temperature, (E) reaction time and (F) pH. Each data point represents the average value from three measurements on the same samples. Error bars show the standard deviations.

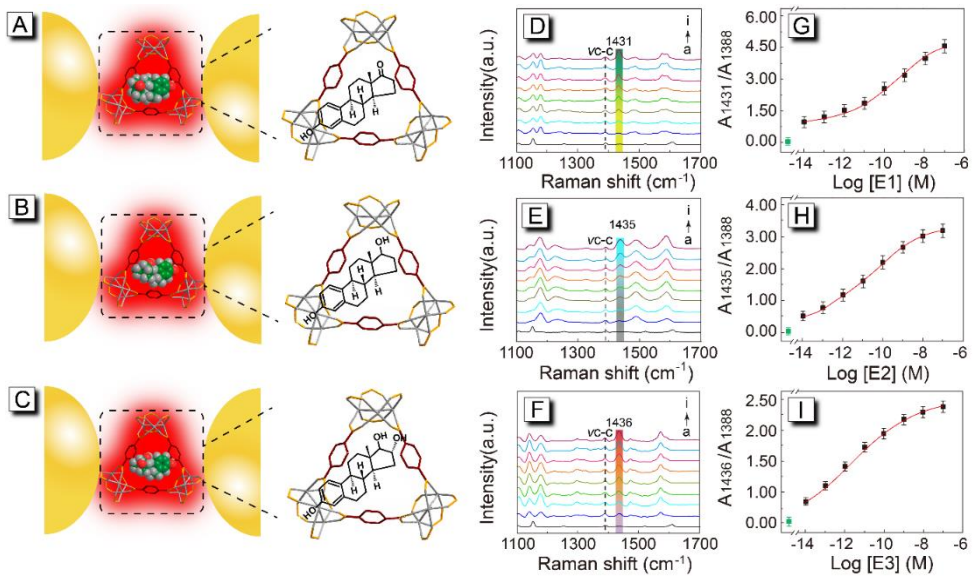

Fig. S14 Schematic diagram of the PMNs-based PDI-SERS strategy for differentiation of (A) E1, (B) E2 and (C) E3. SERS spectra of the PMNs with the presence of (D) E1, (E) E2, (F) E3 at various concentrations (a-i: 0, 10^{-14}, 5×10^{-14}, 10^{-13}, 10^{-12}, 10^{-11}, 10^{-10}, 10^{-9}, 10^{-8}, 10^{-7} M). Plots of (G) I_{1431}/I_{1388}, (H) I_{1435}/I_{1388}, (I) I_{1436}/I_{1388} versus the logarithmic concentrations of E1, E2, E2, respectively (n=6). The green points in Figure 3G-I represent the reference values of the PMNs without presence of PEs.

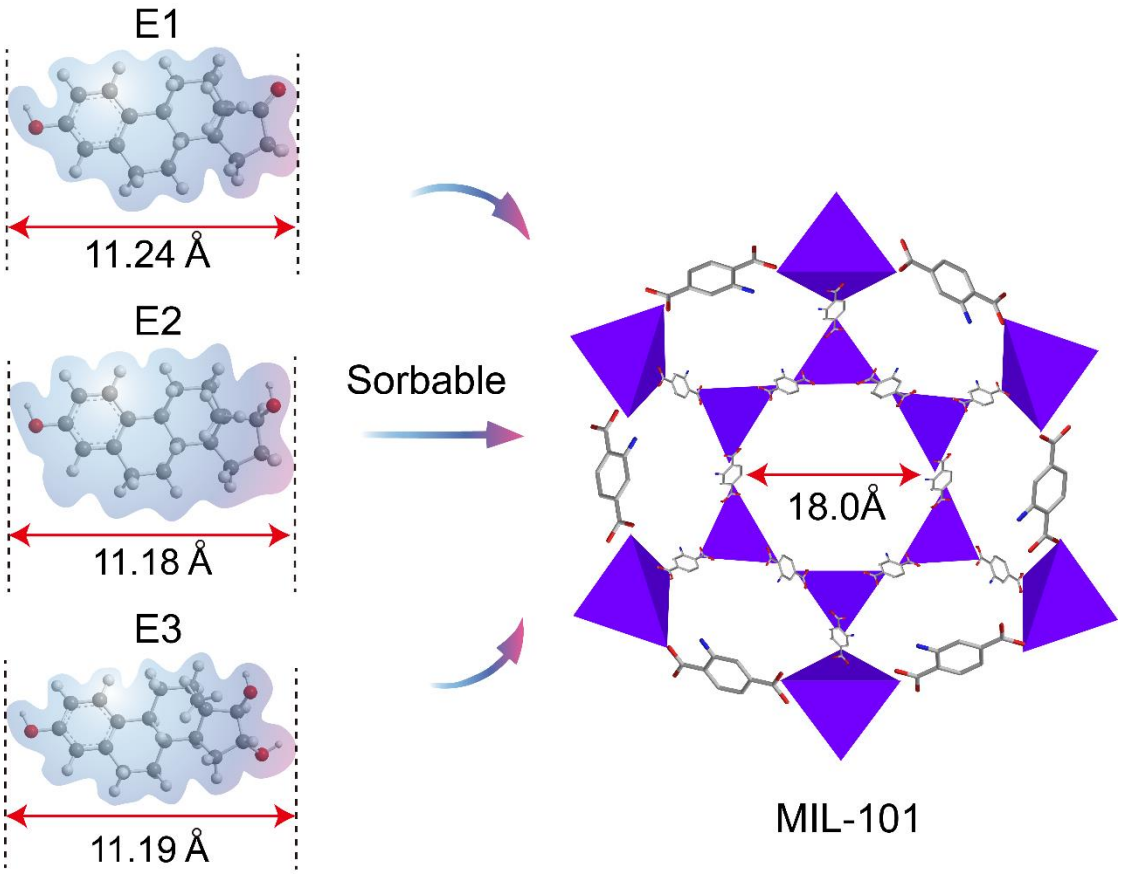

Fig. S15 Molecular kinetic diameters of the PEs molecules and schematic illustrating the interaction of the MIL-101 with PEs by host-guest interactions.

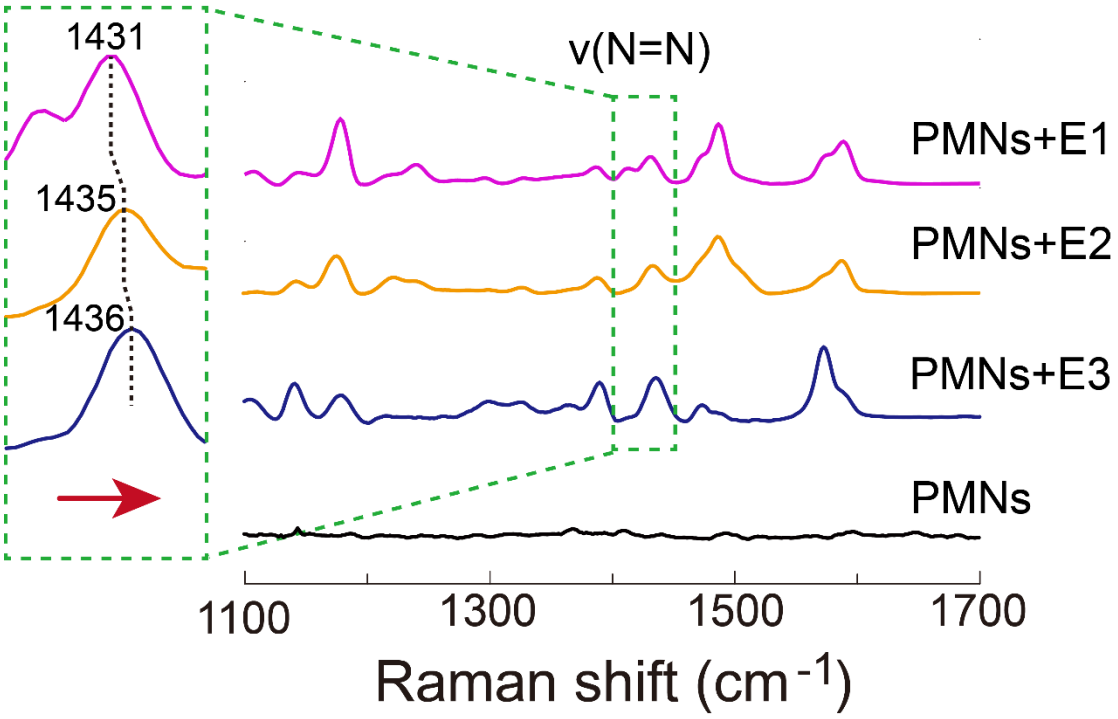

Fig. S16 SERS spectra collected from PMNs before (blank) and after addition of E1, E2 and E3.

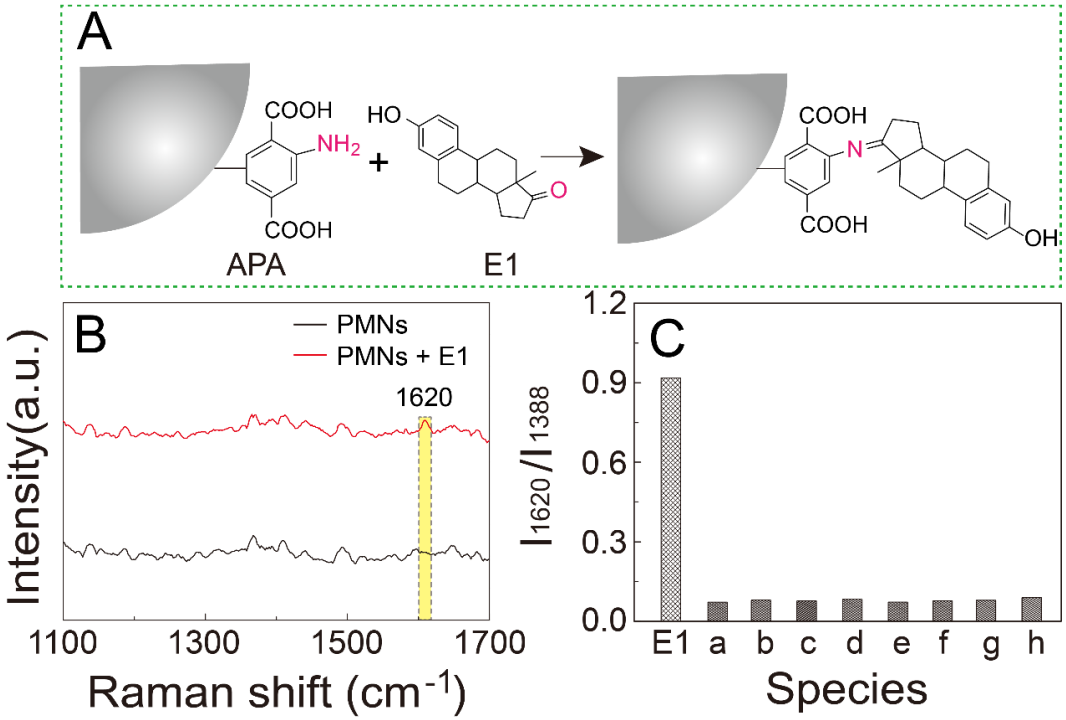

Fig. S17 (A) Schematic illustration of formation of the APA-E1 complex. (B) SERS spectra of the PMNs before (black) and after (red) reacted with E1. (C) Relative intensity ratio of I_{1653}/I_{1338} after exposed to various interferents (a-h: E2, E3, bisphenol A, hexestrol, diethylstilbestrol, ethinylestradiol, estrovis, quinestrol) at 1 mM and E1 at 1 nM.

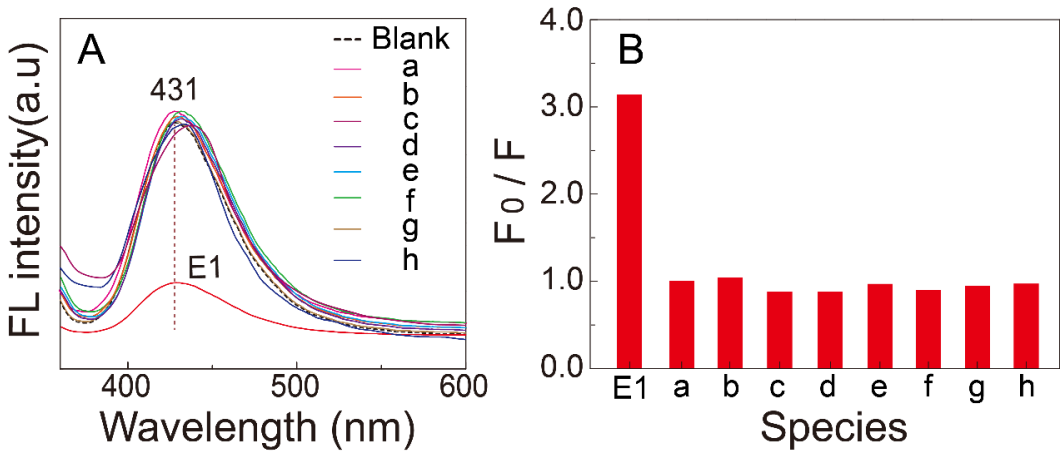

Fig. S18 (A) FL spectra of the PMNs after exposed to various interferents (a-h: E2, E3, bisphenol A, hexestrol, diethylstilbestrol, ethinylestradiol, estrovis, quinestrol) at 1 mM and E1 at 1 nM. (B) Histogram of relative intensity ratio of F_0/F in part (A). F_0 and F are the FL intensity of the PMNs without and with the presence of the analytes, respectively.

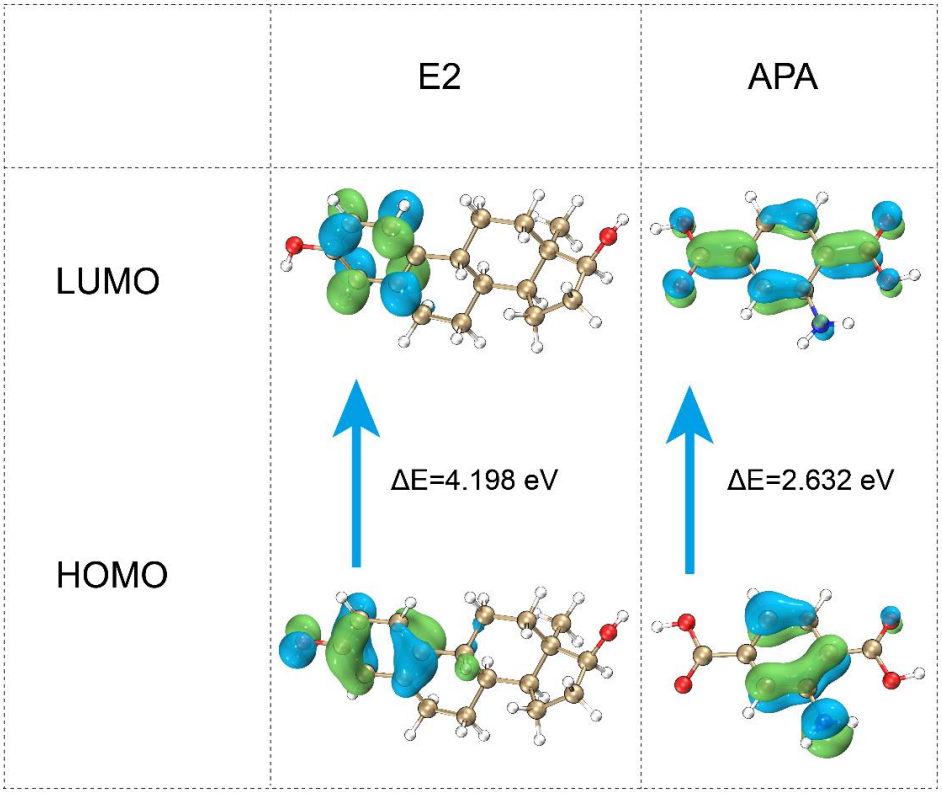

Fig. S19 The HOMO-LUMO energy gap of E2 and APA.

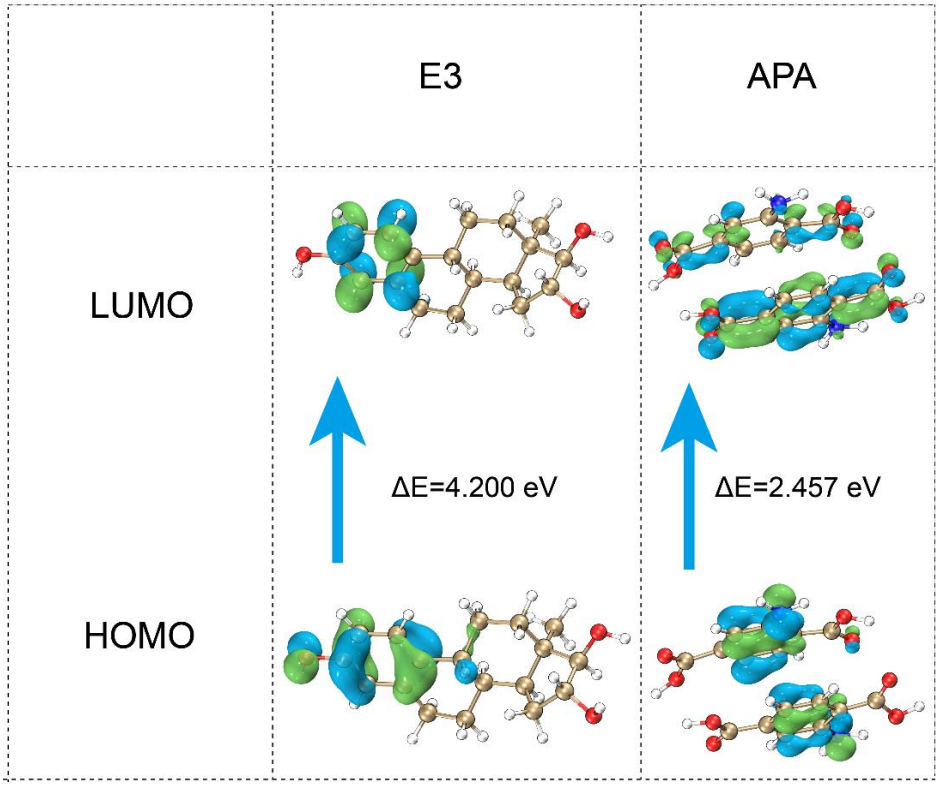

Fig. S20 The HOMO-LUMO energy gap of E3 and APA.

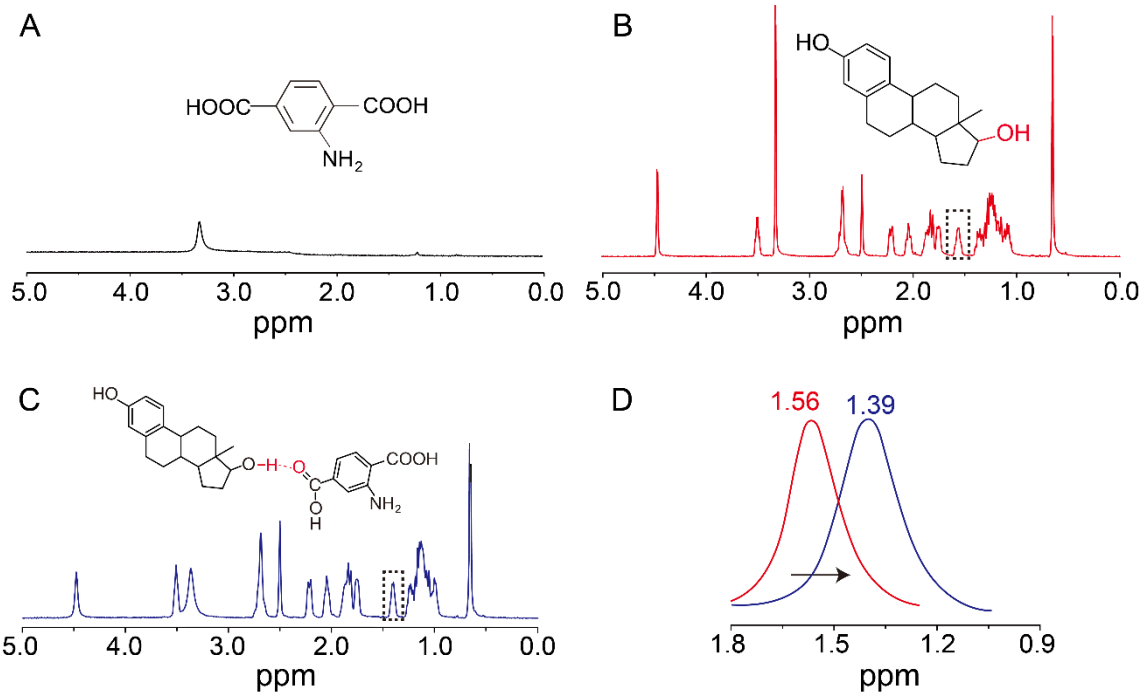

Fig. S21 ^{1}H-NMR spectra of (A) APA, (B) E2, (C) E2-APA complex. (D) Partial ^{1}H NMR spectra from the (B-C).

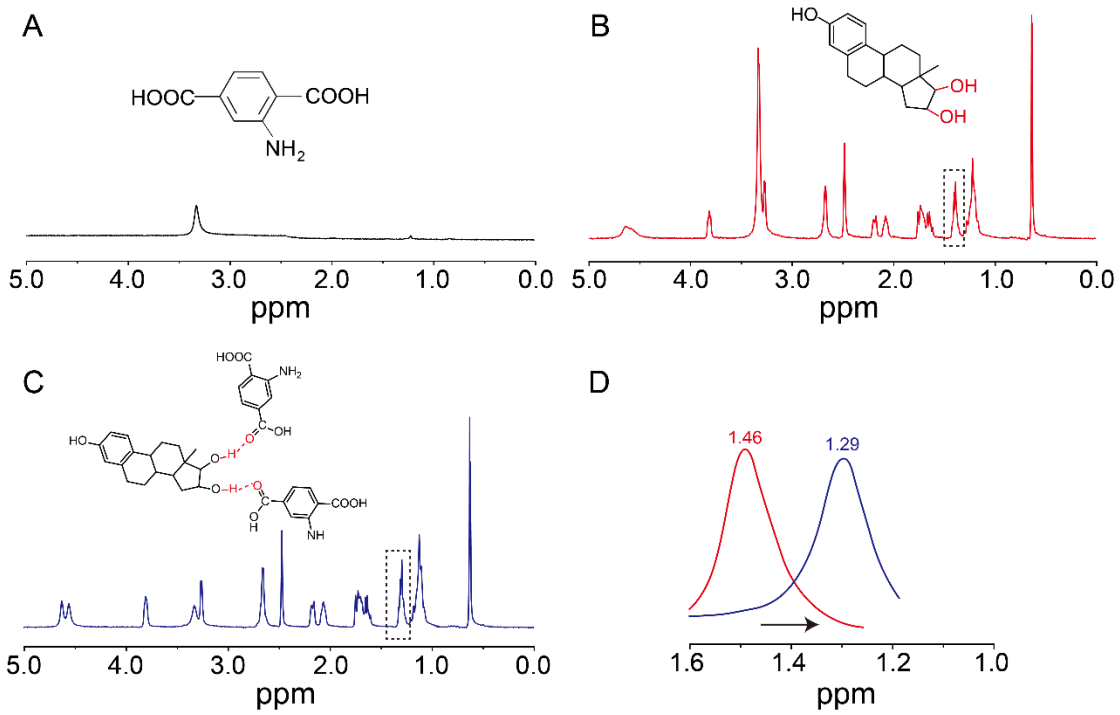

Fig. S22 ^{1}H-NMR spectra of (A) APA, (B) E3, (C) E3-APA complex. (D) Partial ^{1}H NMR spectra from the (B-C).

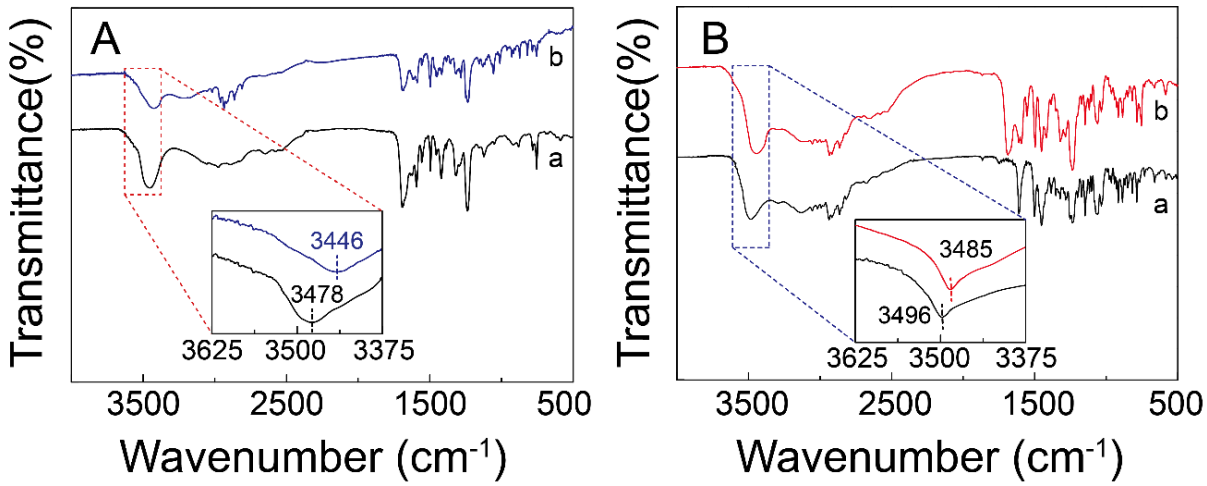

Fig. S23 FTIR spectra of (A) E2 (black line) and E2-APA (red line), (B) E3 (black line) and E3-APA (red line).

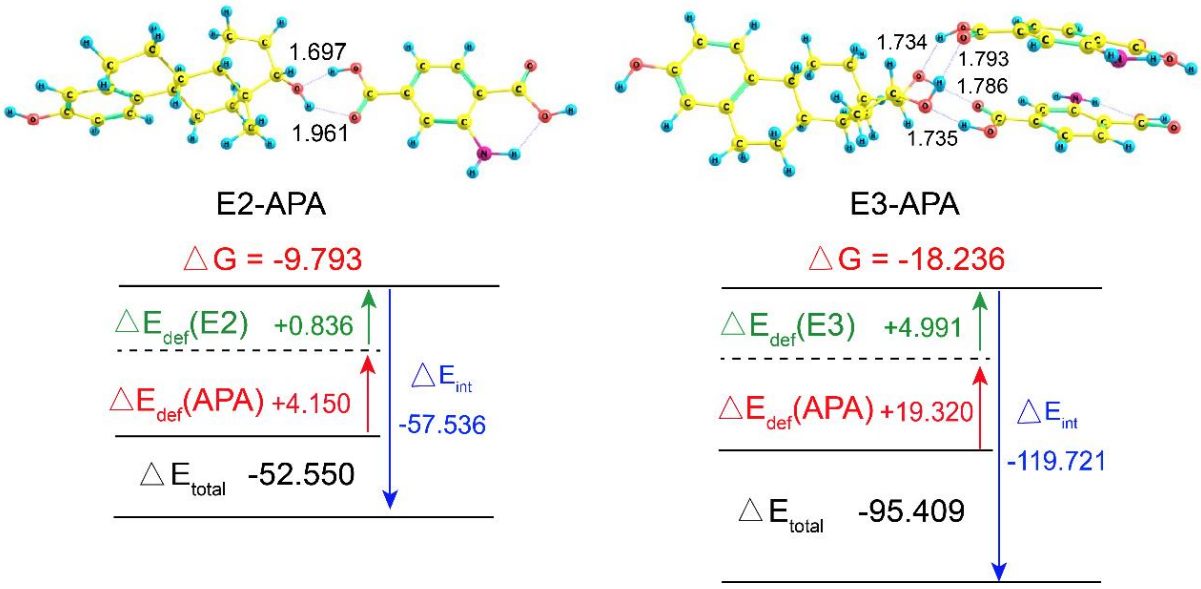

Fig. S24 Geometrical structures (distances in Å) of optimized E2-APA and E3-APA.

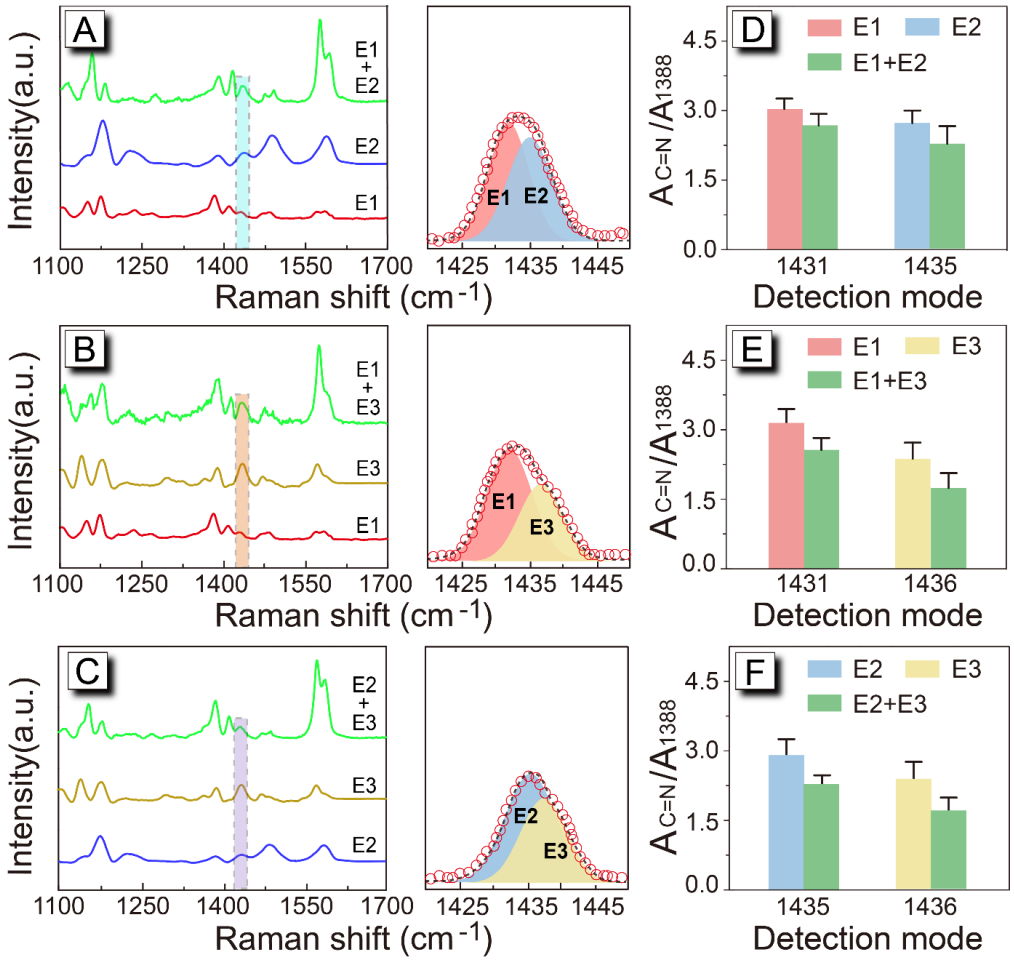

Fig. S25 SERS spectra of the PMNs sensor for (A) simultaneous detection of 1 nM E1 and 1 nM E2, (B) 1 nM E1 and 1 nM E3, (C) 1 nM E2 and 10 nM E3. (D-F) Relative SERS intensities of individual and multiplex of PEs in (A)-(C), respectively. The red curves represent the recorded experimental data.

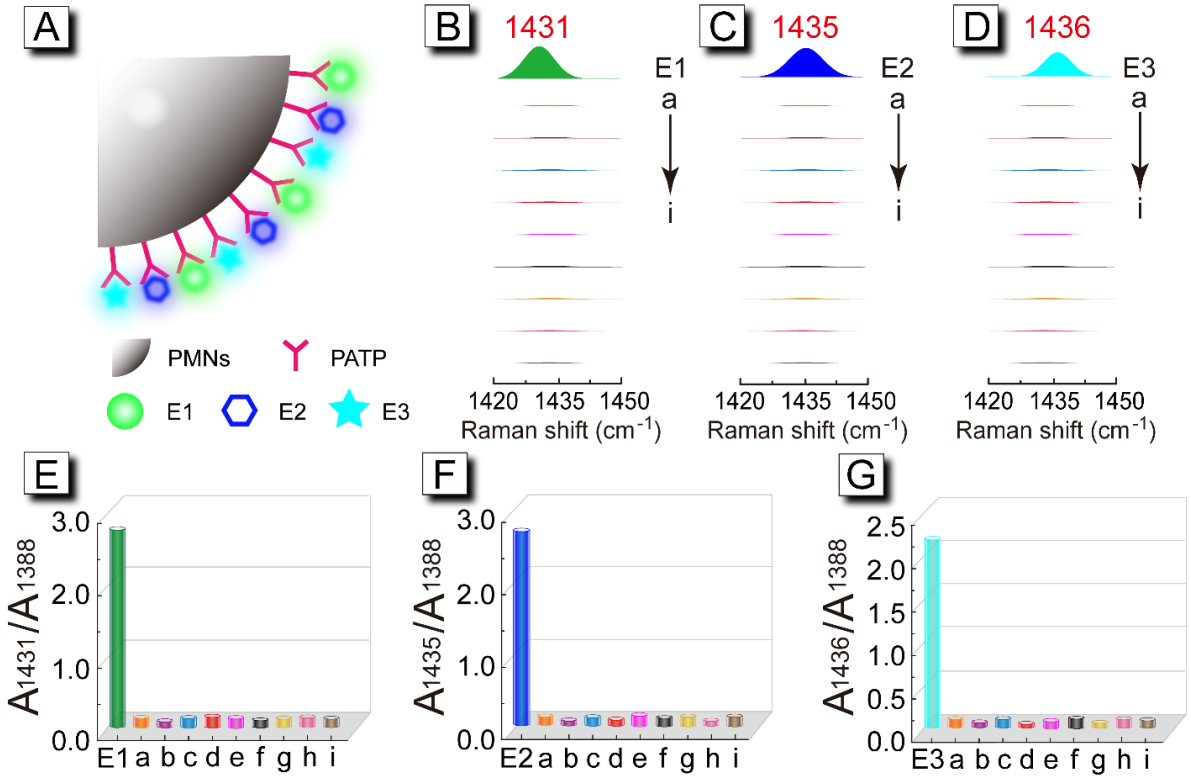

Fig. S26 (A) Schematic representation of the interaction of PMNs with E1, E2 and E3. SERS spectra of PMNs in the presence of (B) E1, (C) E2, (D) E3 at 1 nM and various interfering substances at 1 μM (a-i: quinestrol, epimestrol, nilestriol, estramustine, norgestrel, estradiol benzoate, histidine, estrone acetate and estradiol dipropionate). (E-G) Relative area ratio of A_{1431}/A_{1388}, A_{1435}/A_{1388} and A_{1436}/A_{1388} in part (B-D), respectively.

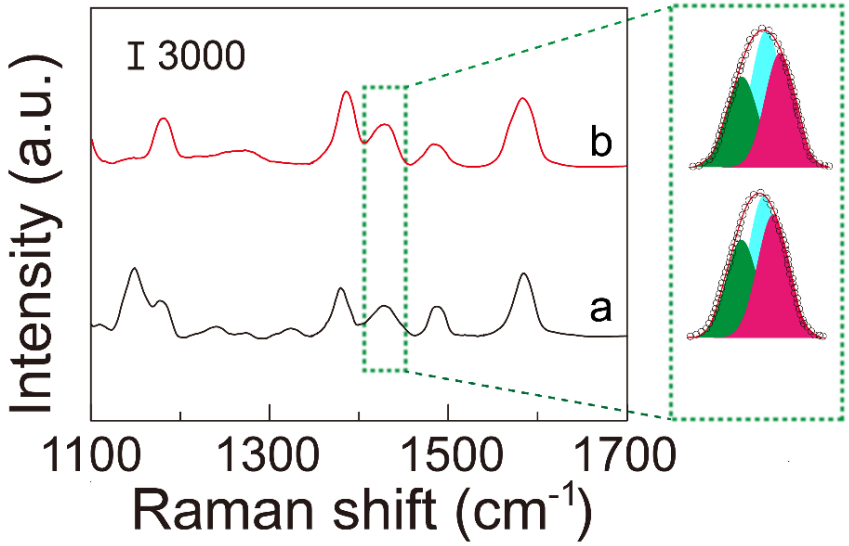

Fig. S27 The detection of the E1, E2 and E3 (1 nM) in the presence of 1 μM potential interfering substances (a), including quinestrol, epimestrol, nilestriol, estramustine, norgestrel, estradiol benzoate, histidine, estrone acetate and estradiol dipropionate. The upper SERS spectrum (b) was the corresponding PMNs reacted with the mixture containing E1, E2 and E3 (1 nM). The green, cyan and pink zones indicate the representative vibration peaks of the E1, E2 and E3, respectively.

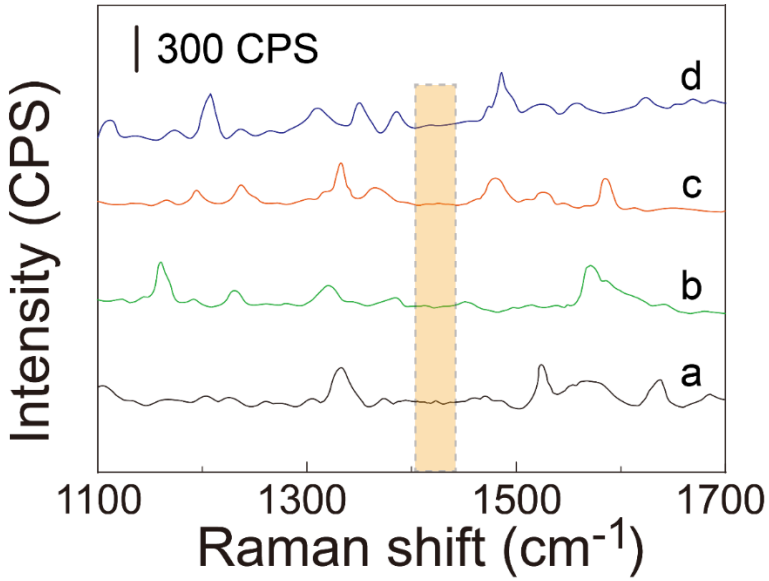

Fig. S28 SERS spectra of PMNs with the presence of (a) milk, (b) fish, (c) duck meat and (d) wastewater specimens. The yellow zone indicates the representative vibration peaks of the PEs. There are no significant SERS signals of PEs among three spectra, indicating that the background matrices have little impact on the SERS detection of PEs.

Table S1 Assignments of SERS Bands of the E1

Raman shift (cm^{-1})	Assignments [a]
1107	δCH ring; γCH
1145	$\delta(CH_3)$
1180	$\gamma(CH_2)$
1217	ν(CN)+δ(CNN); δ(CH) +δ(OH)+ν(CC) from phenol groups
1241	ν(CO); ν(CC) ring
1298	δ(OH)
1326	δ(CCH) + δ(NCC) from phenyl rings
1388	ν(CC) from phenyl rings; δ(CH) + δ(OH) from phenol groups
1412	ν(CC)
1472	δCH_2
1487	$\delta(CH_3)$
1589	ν(CC) ring
1617	ν(CC) ring

[a] ν, stretching
δ, in-plane bending
γ, out of plane bending

Table S2 Assignments of SERS Bands of the E2

Raman shift (cm^{-1})	Assignments [a]
1113	δCH ring; γCH
1143	$\delta(CH_3)$
1176	$\gamma(CH_2)$
1222	ν(CN)+δ(CNN); δ(CH) +δ(OH)+ν(CC) from phenol groups
1242	ν(CO); ν(CC) ring
1300	δ(OH)
1327	δ(CCH) + δ(NCC) from phenyl rings
1388	ν(CC) from phenyl rings; δ(CH) + δ(OH) from phenol groups
1488	$\delta(CH_3)$
1589	ν(CC) ring
1621	ν(CC) ring

[a] ν, stretching
δ, in-plane bending
γ, out of plane bending

Table S3 Assignments of SERS Bands of the E3

Raman shift (cm^{-1})	Assignments [a]
1105	δCH ring; γCH
1142	$\delta(CH_3)$
1178	$\gamma(CH_2)$
1298	δ(OH)
1325	δ(CCH) + δ(NCC) from phenyl rings
1388	ν(CC) from phenyl rings; δ(CH) + δ(OH) from phenol groups
1411	ν(CC)
1474	$\delta(CH_2)$
1487	$\delta(CH_3)$
1589	ν(CC) ring

[a] ν, stretching
δ, in-plane bending
γ, out of plane bending

Table S4 SERS detection limits of three PEs in complex matrices

Samples	LOD (μg/kg)		
	E1	E2	E3
Milk	0.42	0.58	0.72
Fish	0.33	0.51	1.06
Duck	0.29	0.35	0.62
Wastewater	0.12	0.26	0.38

Table S5 Determination of E1 in the complex samples and comparison with HPLC (n=3)

Samples	Spiked (μM)	PDI-SERS			HPLC		
		Found (μM)	R [a] (%)	RSD (%)	Found (μM)	R [b] (%)	RSD (%)
Milk	0	ND [b]	–	–	ND	–	–
	50	43.26	86.51	8.8	45.68	91.36	3.2
	100	92.13	92.13	7.6	96.16	96.16	4.8
Fish	0	ND	–	–	ND	–	–
	50	44.36	88.72	9.1	45.27	90.53	3.8
	100	93.52	93.52	7.8	95.16	95.16	4.3
Duck	0	ND	–	–	ND	–	–
	50	44.71	89.42	9.3	46.85	93.69	4.6
	100	91.54	91.54	6.3	91.65	91.65	5.2
Waster water	0	ND	–	–	ND	–	–
	50	43.59	87.18	7.5	48.61	97.21	5.9
	100	90.82	90.82	6.4	102.5	102.5	4.3

[a] R: recovery of the method
[b] ND: lower than LOD

Table S6 Determination of E2 in the complex samples and comparison with HPLC (n=3)

Samples	Spiked (μM)	PDI-SERS			HPLC		
		Found (μM)	R [a] (%)	RSD (%)	Found (μM)	R [b] (%)	RSD (%)
Milk	0	ND [b]	–	–	ND	–	–
	50	52.81	105.6	10.5	45.65	91.29	5.8
	100	92.61	92.61	9.6	95.35	95.35	3.2
Fish	0	ND	–	–	ND	–	–
	50	45.37	90.73	9.8	46.81	93.62	3.8
	100	95.42	95.42	7.5	90.13	90.13	5.6
Duck	0	ND	–	–	ND	–	–
	50	44.08	88.16	11.2	50.65	101.3	5.1
	100	93.28	93.28	8.9	94.62	94.62	3.5
Waster water	0	ND	–	–	ND	–	–
	50	54.12	108.2	9.1	47.63	95.25	6.3
	100	91.36	91.36	7.8	103.6	103.6	4.2

[a] R: recovery of the method
[b] ND: lower than LOD

Table S7 Determination of E3 in the complex samples and comparison with HPLC (n=3)

Samples	Spiked (μM)	PDI-SERS			HPLC		
		Found (μM)	R [a] (%)	RSD (%)	Found (μM)	R [b] (%)	RSD (%)
Milk	0	ND [b]	–	–	ND	–	–
	50	45.26	90.52	9.2	38.42	92.83	4.7
	100	93.44	93.44	8.6	96.41	96.41	3.1
Fish	0	ND	–	–	ND	–	–
	50	49.11	98.22	7.4	40.21	103.2	5.2
	100	92.89	92.89	5.9	95.18	95.18	4.3
Duck	0	ND	–	–	ND	–	–
	50	47.21	94.42	8.4	41.32	95.26	6.8
	100	90.17	90.17	8.2	92.53	92.53	5.2
Waster water	0	ND	–	–	ND	–	–
	50	54.88	109.8	10.5	37.34	93.65	5.8
	100	92.48	92.48	9.3	102.8	102.8	3.2

[a] R: recovery of the method
[b] ND: lower than LOD

Table S8 Comparing the detection performance of different methods for PEs sensing

Methods	Materials	Targets	Linearity (nM)	LOD (nM)	References
Fluorescence	Ru-QDs	E2	80-400	37	7
Fluorescence	Fe_3O_4@MIPs	E2	100-7000	30	8
Fluorescence	Fe_3O_4@SiO_2-Dye-MIPs	E2	1000-20000	190	9
Electrochemistry	Pt/Se/RD	E2	50-85000	11	10
Electrochemistry	CuPc-P6LC-Nafion	E2	80-7300	5	11
Electrochemistry	Fe_3O_4-MIP/SPCE	E2	50-10000	20	12
Electrochemistry	rGO-AgNPs	E3	100-3000	21	13
SERS	Au@Ag NPs	E2	10^{-4}-1	10^{-6}	14
SERS	Au@Ag CS NPs	E2	10^{-4}-10	$5x10^{-5}$	15
SERS	Au@Ag CS NPs	E1/E2	0.01-50	0.005	16
SERS	PMNs	E1/E2/E3	10^{-5}-100	$2x10^{-6}$/$4x10^{-6}$/$6x10^{-6}$	This Work

References

[1] N. R. Jana, L. Gearheart and C. Murphy, *J. Chem. Commun.* 2001, **7**, 617-618.

[2] Z. P. Xia, D. Li and W. Deng, *Anal. Chem.* 2021, **93**, 4924-4931.

[3] Y. W. Zhou and Y. F. Wu, *Compos. Struct*. 2012, **94**, 580-592.

[4] M. Fioravante, A. Shook, I. Thorpe and P. Rheingans, *Comp. Graph. Forum.* 2013, **32**, 311-320.

[5] P. B. Johnson and R. W. Christy, *Phys. Rev.* 1972, **6**, 4370-4379.

[6] A. G. Márquez, A. Demessence, A. E. Platero-Prats, D. Heurtaux, P. Horcajada, C. Serre, J. S. Chang, G. Férey, V. A. de la Peña-O'Shea, C. Boissière, D. Grosso and C. Sanchez, *Eur J. Inorg. Chem.* 2012, **32**, 5165-5174.

[7] H. L. Huang, S. Shi, X. Gao, R. R. Gao, Y. Zhu, X. W. Wu, R. M. Zang and T. M. Yao, *Biosens. Bioelectron.* 2016, **79**, 198-204.

[8] W. N. Ming, X. Y. Wang, W. H. Lu, Z. Zhang, X. L. Song, J. H. Li and L. X. Chen, *Sens. Actuators B Chem.* 2017, **238**, 1309-1315.

[9] Y. Li, C. K. Dong, J. Chu, J. Y. Qi and X. Li, *Nanoscale.* 2011, **3**, 280-287.

[10] A. J. J. Amalraj, U. N. Murthy and S. F. Wang, *ACS Appl. Nano Mater.* 2022, **5**, 1944-1957.

[11] A. Wong, A. M. Santos, E. L. Fava, O. Fatibello-Filho and M. D. P. T. Sotomayor, *Microchem. J.* 2019, **147**, 365-373.

[12] A. A. Lahcen, A. A. Baleg, P. Baker, E. Iwuoha and A. Amine, *Sens. Actuators B Chem.* 2017, **241**, 698-705.

[13] C. A. Donini, M. K. L. da Silva, R. P. Simões and I. Cesarino, *J. Electroanal. Chem.* 2018, **809**, 67-73.

[14] H. B. Pu, X. H. Xie, D. W. Sun, Q. Y. Wei and Y. F. Jiang, *Talanta*. 2019, **195**, 419-425.
[15] S. Y. Liu, R. J. Cheng, Y. Q. Chen, H. J. Shi and G. H. Zhao, *Sens. Actuators B Chem.* 2018, **254**, 1157-1164.
[16] S. Y. Liu, Y. Q. Chen, Y. Wang and G. H. Zhao, *Anal. Chem.* 2019, **91**, 7639-7647.